IEEE Access
Multidisciplinary ⋮ Rapid Review ⋮ Open Access Journal

Received January 18, 2018, accepted February 20, 2018, date of publication February 28, 2018, date of current version April 23, 2018.

Digital Object Identifier 10.1109/ACCESS.2018.2810262

Low-Scattering Tri-Band Metasurface Using Combination of Diffusion, Absorption and Cancellation

YAQIANG ZHUANG[1], GUANGMING WANG[1], (Member, IEEE), QINGFENG ZHANG[2], (Senior Member, IEEE), AND CHENG ZHOU[3]

[1]Air and Missile Defense College, Air Force Engineering University, Xi'an 710051, China
[2]Department of Electrical and Electronic Engineering, Southern University of Science and Technology, Shenzhen 518055, China
[3]Unit 95899 of CPLA, Beijing 100085, China

Corresponding authors: Guangming Wang (wgming01@sina.com) and Qingfeng Zhang (zhangqf@sustc.edu.cn)

This work was supported in part by the National Natural Science Foundation of China under Grant 61601498, in part by the Guangdong Natural Science Funds for Distinguished Young Scholar under Grant 2015A030306032, in part by the Guangdong Special Support Program under Grant 2016TQ03X839, in part by the Shenzhen Science and Technology Innovation Committee funds under Grant KQJSCX20160226193445, Grant JCYJ20150331101823678, Grant KQCX201503311 0182368, Grant JCYJ20160301113918121, and Grant JSGG20160427105120572, and in part by the Shenzhen Development and Reform Commission Funds under Grant [2015] 944.

ABSTRACT In this paper, we proposed for the first time a novel mechanism to design a tri-band low-scattering metasurface. The radar cross section (RCS) reduction in the three operational bands relies on scattering diffusion, absorption, and scattering cancellation, respectively. The diffusion metasurface was realized by distributing scattering unit cells with different rotation angles. For the absorption, four units operating at different frequencies were combined to achieve a broadband absorption. The scattering cancellation was realized by arranging two out of phase elements in a chessboard configuration. The tri-band metasurface was constructed by directly combining the three metasurfaces in a single assembly. The simulated and measured results have a good agreement. The tri-band RCS reduction is well preserved up to 45° with polarization-independent performance. This paper provides an alternative approach to design the multi-band metasurface for stealth application.

INDEX TERMS Metasurface, tri-band, radar cross section reduction, diffusion, absorption, scattering cancellation.

I. INTRODUCTION

Design of low-scattering platforms attracts more and more attentions due to the increasing demand of stealth technology in military applications. Reduction of radar cross section (RCS) is an important part of the stealth technology [1]. The conventional radar stealth technology relies on either shaping configurations or loading radar absorbing materials (RAMs) [1], which suffer from design complexity and bulky volume. Recently, metasurface was proposed to arbitrarily manipulate electromagnetic (EM) waves with low loss, low profile and broadband performance [2]–[4]. Using metasurface for RCS reduction has become a hot research topic recently. There are two kinds of metasurface-based technologies: absorption [5]–[8] and scattering control [9]–[27]. The low-scattering metasurfaces have been comprehensively investigated from gigahertz to terahertz regime for both planar and conformal cases. The ultra-thin metamaterial absorber dissipated energy into the dielectric at resonance frequencies [5], and the working bandwidth was further enhanced by loading lumped elements [6]–[8]. The scattering control for RCS reduction based on either scattering cancellation [9]–[13] or diffusion [14]–[23]. The scattering cancellation is achieved by arranging two out of phase unit cells in chessboard-like configuration, which can diminish specular reflection and redirect energies into diagonal and off-diagonal directions [9]–[13]. To mimic a diffusion process, the metasurface with random phase distribution can disperse incoming EM waves into various directions [14]–[23]. The desirable diffusion scattering can be realized by combing the coding concept and optimization algorithm [24]–[26], which are usually time-consuming in design, especially for a multi-bit coding metasurface. An easy and efficient strategy was proposed to design diffusion metasurface using a random combination of gradient subarrays with different gradient directions [27]. However, all the above mentioned metasurfaces reduce RCS in a single band only. Some dual-band metasurfaces have been investigated later for RCS reduction [28]–[30]. The RCS reduction in two operational bands relies on either anomalous reflection [28] or scattering cancellation [29]. The two operational bands in this kind of dual-band metasurfaces can be influenced by each other, leading to a limited frequency ratio. A dual-band low-scattering metasurface was later designed using a combination of two single-band metasurfaces based on absorption and diffusion, respectively [30]. The influence between two operational bands is independent in this case. To date, the tri-band metasurface for RCS reduction is still not explored and reported.

In this paper, we proposed a tri-band metasurface for RCS reduction. The three operational bands operate using scattering diffusion, absorption and scattering cancellation, respectively. The underlying working mechanisms of each operational band are quite different, and the three bands have little influence on each other. To realize the diffusion scattering performance, we use an ultra-wideband polarization rotation unit cell as the basic coding meta-atom, and the phase distribution was optimized with the aid of a hybrid algorithm. In the absorption case, we adopt four unit cells as a supercell to enhance the absorption bandwidth. The proposed low-scattering metasurface features tri-band, wide-angle and polarization-independent performance.

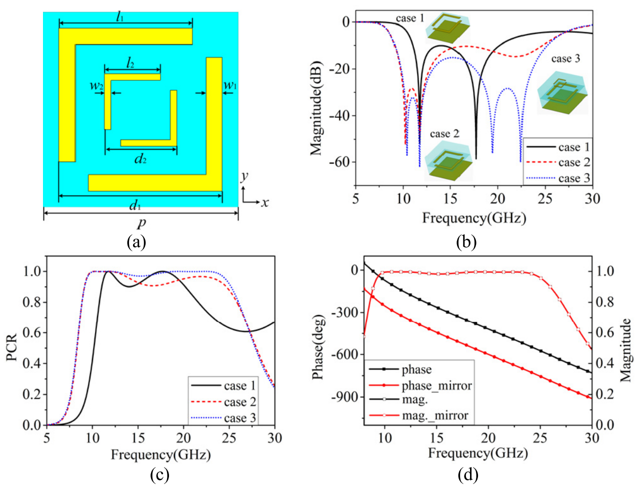

FIGURE 1. (a)The front view of the polarization rotatable unit cell; (b) the co-polarized reflection magnitudes and (c) PCRs of three cases; (d) the cross-polarized reflection coefficients of the unit cell and its mirror counterpart.

II. UNIT CELL DESIGN

A. ULTRA-WIDEBAND POLARIZATION ROTATABLE UNIT CELL

The polarization rotatable unit cell, as illustrated in Fig. 1(a), is composed of three metallic layers and two dielectric layers. Both two metallic patterns comprised of a pair of L-shaped structure. The two identical dielectric layers have a dielectric constant of 2.2, a thickness of 2 mm and a tangent loss of 0.006. The structural parameters are optimized as $p = 6$ mm, $w_1 = 0.5$ mm, $l_1 = 4.1$ mm, $d_1 = 5$ mm, $w_2 = 0.2$ mm, $l_2 = 1.7$ mm and $d_2 = 2.2$ mm. Here, the dual-layer configuration enhances the bandwidth as well as the polarization conversion ratio (PCR). To show the bandwidth and efficiency enhancement of the proposed dual-layer unit cell, the co-polarized reflection magnitudes and PCRs of three different cases are depicted in Fig. 1(b) and (c). The detail structures of the three cases are shown in the inset of Fig. 1(b). Note that the co-polarized reflection magnitude is below −10 dB from 11 GHz to 20.2 GHz for case 1. In case 2, the bandwidth is enhanced to 9.1-24.7 GHz after covering a superstrate, as presented by red dashed line. It is clearly observed that the reflection magnitude is between −15 dB and −10 dB from 13.6 GHz to 24.7 GHz, indicating that the PCR is less than 0.95 within this bandwidth. To further improve the PCR, another pair of L-shaped structure was printed on the superstrate as the case 3. The reflection magnitude is below −15 dB from 9.1 GHz to 25.2 GHz, and the PCR is higher than 0.95 within the whole bandwidth, revealing that the incident polarization is converted into its orthogonal polarization with high efficiency. In other words, the polarization rotatable unit cell can achieve a +90° polarization conversion of incident EM wave. Analogously, the mirror counterpart of the unit cell can provides a −90° polarization rotation with the same amplitude. Therefore, the cross-polarized reflection phase of the unit cell is strictly out of phase with its mirror counterpart and the reflection magnitudes are greater than 0.95 from 9.2 GHz to 25.2 GHz, as shown in Fig. 1(d). Thus, the proposed unit cell and its mirror counterpart can be employed as the basic meta-atoms of a 1-bit coding metasurface.

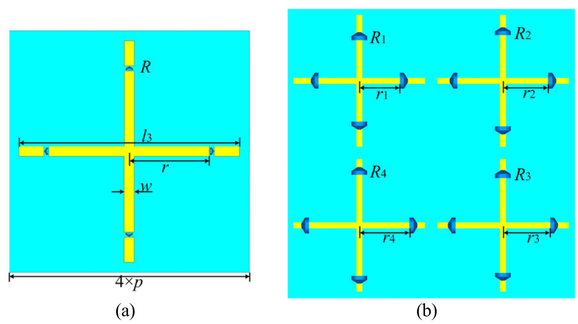

FIGURE 2. The schematic of (a) absorption unit cell and (b) absorption supercell.

B. BROADBAND ABSORPTION SUPERCELL

As shown in Fig. 2(a), the absorption unit cell has a sandwich-like structure, namely, a top metallic structure, a middle F4B substrate with a thickness of 4 mm and a dielectric constant of 2.2, and a bottom metallic ground. The optimum dimensions of the unit cell are $l_3 = 22$ mm, $w = 1$ mm. The effects of the loading position and resistance were investigated firstly. As shown in the Fig. 3(a), the absorption frequency

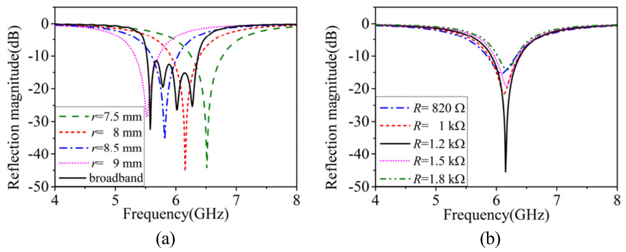

FIGURE 3. **The reflection magnitudes (a) with different loading positions and (b) with different resistances.**

can be manipulated by changing the loading position. One can clearly find that the absorption frequency is decreasing with the increment of parameter r. In addition, the absorption performance was affected by the values of resistors. Note from Fig. 3(b), the best absorption performance can be obtained when the resistance is 1.2 kΩ. However, the 10 dB fractional bandwidth of absorption unit cell is only about 7%, which is a little narrow. To enhance the absorption bandwidth, we combined four unit cells working at adjacent frequencies to be an absorption supercell, as shown in Fig. 2(b). The initial loading positions are 7.5 mm, 8 mm, 8.5 mm, and 9 mm, and the initial resistances are 1.2 kΩ. Due to the coupling between adjacent unit cells, both the loading position and resistance should be optimized to achieve preferred broadband performance. The final optimum positions are $r_1 = 7.2$ mm, $r_2 = 8$ mm, $r_3 = 8.3$ mm, and $r_4 = 8.8$ mm, and resistances are $R_1 = 2.7$ kΩ, $R_2 = 1.5$ kΩ, $R_3 = 4.7$ kΩ, and $R_4 = 4.7$ kΩ. The reflection magnitude is below −10 dB from to 5.52 GHz to 6.37 GHz, as shown by black solid line in Fig. 3(a). It is clearly seen that the fractional bandwidth has been enhanced to 14.3% in C-band by combining four neighboring absorption frequencies.

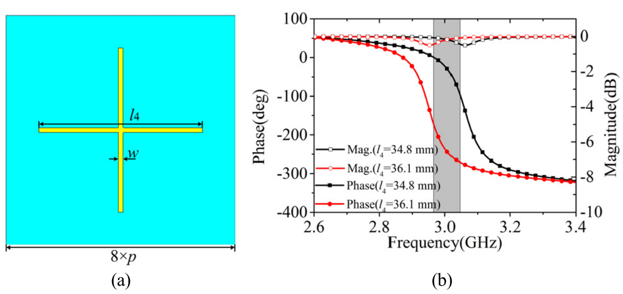

FIGURE 4. **(a) The schematic of crossed dipole for scattering cancellation and (b) the reflection coefficients for l4=34.8 mm and l4=36.1 mm.**

C. CROSSED DIPOLE FOR SCATTERING CANCELLATION

To reduce RCS in S-band based on scattering cancellation, we still use crossed dipole as the basic meta-atom, as shown in Fig. 4(a). The substrate layer is identical to that of the absorption unit cell. To realize 10 dB RCS reduction, the phase difference between two basic meta-atoms should be 180° ± 37°, while the magnitudes should be equal to each other [8]. The reflection phase can be tuned by changing the parameter l_4, and 180° ± 37° phase difference was achieved when l_4 = 34.8 mm and 36.1 mm from 2.95 GHz to 3.06 GHz. Moreover, as shown in Fig. 4(b), almost total reflection is achieved due to the metallic ground on the back. The maximum phase difference (217°) is set at the center frequency 3 GHz to enhance the operational bandwidth. As a result, a metasurface constructed by arranging one type of crossed dipoles surrounded by the other type will achieve a null in boresight direction due to destructive interference around 3 GHz.

III. OVERALL METASURFACE DESIGN

A. DESIGN PRINCIPLE

The scattering pattern of metasurface for scattering manipulation illuminated by plane wave can be regarded as the radiation pattern of an array. Thus, the scattering pattern can be theoretically calculated by using array theory. The scattering pattern of the whole metasurface was the composition of the contributions of all the elements, and is generally expressed as

$$\vec{E}_{total} = \sum_{m=1}^{M}\sum_{n=1}^{N}\vec{E}_{m,n} \times \exp\left[jk_0\left(md_x\sin\theta\cos\varphi + nd_y\sin\theta\sin\varphi\right)\right] \quad (1)$$

where $\vec{E}_{m,n}$ is the electric far-field pattern of the element (m, n), and expressed by $\vec{E}_{m,n} = \vec{E}_1\exp(j\varphi_{mn})$, where $\vec{E}_1$ is the electric far-field pattern of the basic element and φ_{mn} is the relative phase of the element (m, n). θ and φ are the elevation and azimuth angles, respectively; d_x and d_y denote the element period along the x and y directions, respectively; k_0 is the wave number in free space. Substituting $\vec{E}_{m,n} = \vec{E}_1\exp(j\varphi_{mn})$ into Eq. (1) leads to

$$\begin{aligned}\vec{E}_{total} &= \vec{E}_1\sum_{m}\sum_{n}\exp\left[j\left(\varphi_{mn} + k_0md_x\sin\theta\cos\varphi + k_0nd_y\sin\theta\sin\varphi\right)\right] \\ &= \vec{E}_1\cdot AF \end{aligned} \quad (2)$$

where AF is the array factor. Accordingly, the scattering pattern is determined by the element phase distribution. To diffuse the scattering into numerous directions, the simplest method is to generate a random phase matrix to determine the diffusion metasurface configuration. However, this method cannot guarantee an optimal result. One method to solve this issue is to use an optimization algorithm to find the optimal coding phase matrix.

Simulated Annealing algorithm is a method for local searching proposed by Kirkpatrick et al. [31]. It has advantages of simple description and high efficiency. It begins with an initial solution that is randomly modified in an iterative process. The main parameters of Simulated Annealing algorithm are the initial temperature T, the decreasing rate in each iteration α, the final temperature T_f, the number of iterations I and the merit function. The goal of the optimization is to find an optimal coding matrix (M_{opt}) that results in the smallest maximum value of the scattered fields. Therefore, the merit

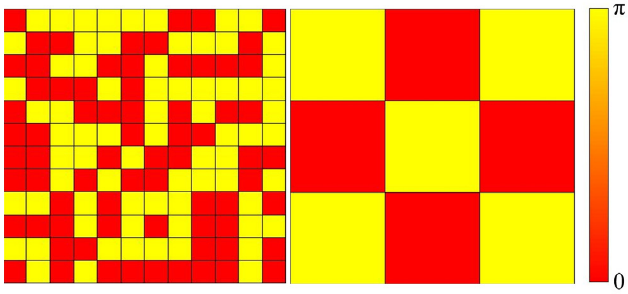

FIGURE 5. The phase distribution of optimal diffusion metasurface (left) and chessboard metasurface (right).

function can be expressed by $F(M_{opt}) = \min(AF_{max})$, where AF_{max} is the maximum value of AF corresponding to given coding matrix. In our case, the size of the coding matrix is 12×12, and the element of the matrix is either 0 or π. One should note that the numbers of 0 is equal to that of π, leading to the information entropy of the coding matrix reaches maximum [32]. Moreover, the parameters T, α, T_f and I are set as 100, 0.9, 0 and 500, respectively. The optimal coding matrix is shown in the left part of Fig. 5, and the corresponding theoretical scattering pattern is depicted in Fig. 6(a). It can be clearly seen that the scattered energy has been diffused into numerous directions, leading to both monostatic and bistatic RCS reduction due to the energy conversation.

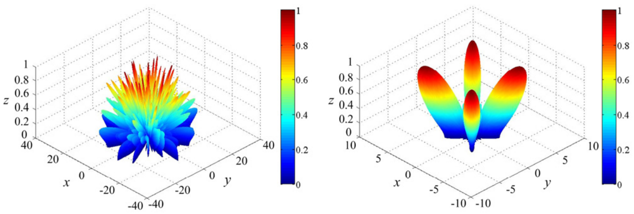

FIGURE 6. The theoretical results of 3D scattering patterns for (a) diffusion metasurface and (b) chessboard metasurface.

The phase distribution for scattering cancellation is shown in the right part of Fig. 5. As seen, 0 and π is intersected with each other to form a chessboard configuration. Fig. 6(b) shows the scattering pattern of the chessboard metasurface. Note that the backward reflection is diminished and four scattered beams occur along diagonal and off-diagonal directions.

B. CONFIGURATION

Based on the proposed three kinds of unit cells and the design principle, we design three individual metasurfaces. Firstly, the diffusion metasurface was designed based on the proposed polarization rotatable unit cell and the optimal coding matrix. Due to fact that the coupling between adjacent unit cells in the random distribution is different from the boundary applied in the unit cell simulation, each diffusion supercell is formed by 4×4 identical unit cells to reduce this effect. Thus, the diffusion metasurface constructed by 48×48 unit cells, which occupies a size of 288×288 mm^2. Secondly, the absorber array was built by periodically distributing the broadband absorption supercells. The absorber array contains 6×6 broadband absorption supercells, leading to the same size as the diffusion metasuface. Thirdly, we also employ 2×2 crossed dipoles as a basic element in designing the chessboard configuration. Therefore, the chessboard metasurface contains 6×6 crossed dipoles with a size of 288×288 mm^2. Finally, the tri-band metasurface for RCS reduction was constructed by directly combining the three individual metasurfaces, the upper-left part of the tri-band metasurface was shown in the Fig. 7, which contains 2×2 diffusion supercells, an absorption supercell and a crossed dipole.

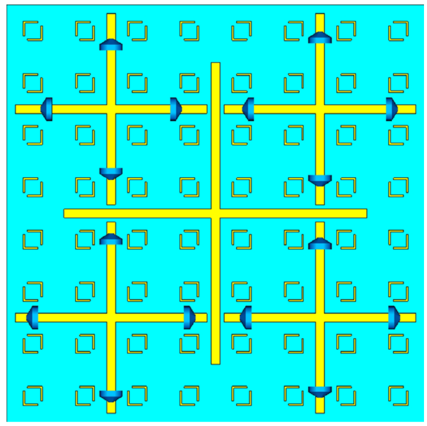

FIGURE 7. The schematic of the upper-left part of the tri-band metasurface.

IV. NUMERICAL AND EXPERIMENTAL RESULTS

A. NUMERICAL RESULTS

Both three individual metasurfaces and tri-band metasurface are simulated in CST Microwave Studio. Only *x*-polarized incidence is considered in the individual metasurface simulation. A metallic plate with the same size is introduced as the reference to show the RCS reduction performance. Fig. 8(a) depicts the RCS reductions of three individual metasurfaces. As expected, the diffusion metasurface can reduce RCS more than 10 dB from 9.5 GHz to 25.1 GHz, which is consistent with the bandwidth of the co-polarized reflection magnitude less than -10 dB. The red dashed line denotes the RCS reduction performance of the absorber array, proving that the RCS of the absorber array is less than that of the metallic plate by more than 10 dB within 5.64-6.4 GHz. The RCS reduction performance of chessboard metasurface was presented by the blue dotted line, showing that the 10 dB RCS reduction can be obtained within 2.96-3.06 GHz, which agrees with the effective phase difference bandwidth (2.95-3.06 GHz). Fig. 8(b) gives the RCS of the tri-band metasurface under illumination by both *x*- and *y*-polarized plane waves. It can be referred from Fig. 8(b) that RCS can be reduced by more than 10 dB within 2.92-3 GHz, 5.57-6.3 GHz and 9.5-25.5 GHz. It is interesting to find that the operational bandwidth of tri-band metasurface is consistent with the operational bands of three

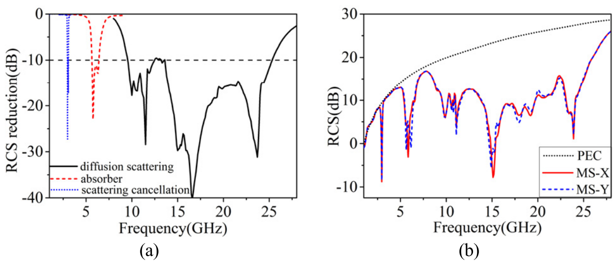

FIGURE 8. (a) The RCS reduction of three individual metasurfaces and (b) the RCS response tri-band metasurface for both x- and y-polarized incidence.

individual metasurfaces, revealing that each RCS reduction mechanism is little affected by other mechanisms. In addition, the RCS reduction performance for x-polarized incidence is similar to that of y-polarized incidence, proving that the tri-band metasurface features polarization-independence.

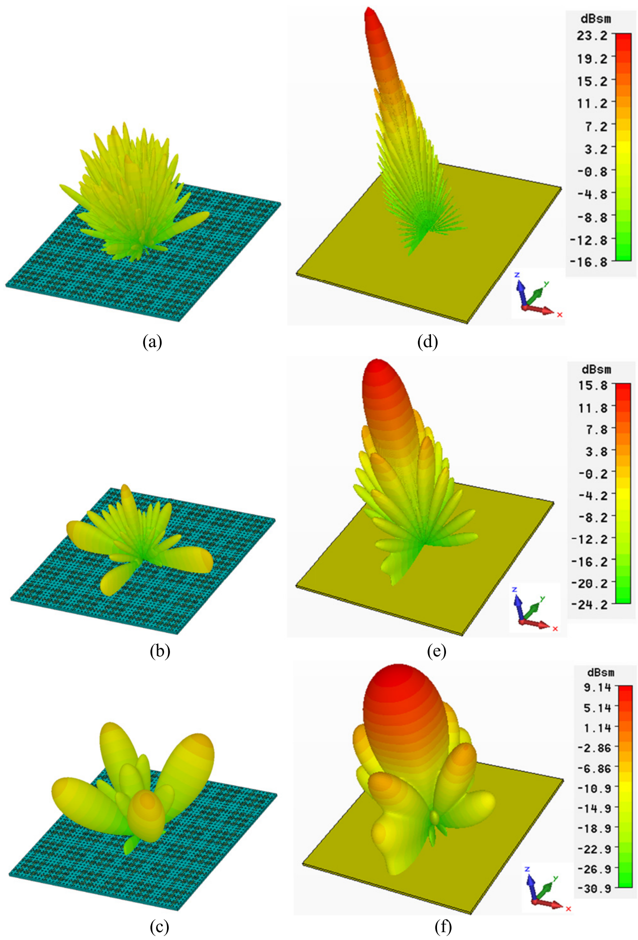

FIGURE 9. 3-D scattering patterns of (a-c) the tri-band metasurface and (d-f) metallic plate at (a, d) 14.9 GHz; (b, e) 6.14 GHz and (c, f) 2.96 GHz.

To better illustrate the underlying mechanisms at three operational bands, we further investigate the three dimensional (3-D) scattering patterns at three frequencies where the best reductions occur, as shown in Fig. 9. The scattering patterns of metallic plate in the same color map scale are also given for comparison. Obviously, the maximum scattered intensities of metasurface are lower than that of the metallic plate. As expected, a diffusion scattering is realized at high frequency, the incident EM wave was absorbed at middle frequency, and the specular reflection can be diminished at low frequency. Moreover, the simulated 3-D scattering patterns at high and low frequencies are consistent with the theoretical results in Fig. 6. As a comparison, the specular reflection occurs at three frequencies for the metallic plate. It is worth noting that though the scattered intensity of metasurface gets enhanced at some directions, the values are too small to be detected.

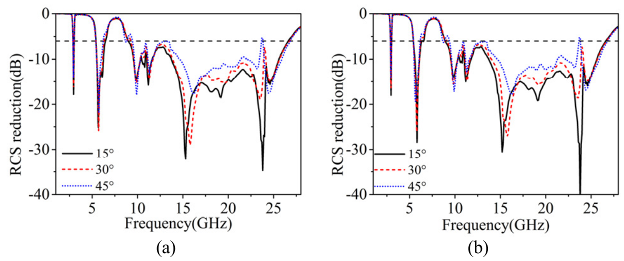

FIGURE 10. The RCS reductions under oblique incidence for (a) x-polarized and (b) y-polarized.

To provide a comprehensive investigation about the angular performance of the proposed metasurface, the RCS reductions under oblique angles are simulated and shown in the Fig. 10. Note that though the RCS reduction performance degrade due to the alteration of phase response at high frequency range, a tri-band RCS reduction is realized for both x- and y-polarized until the incident angle up to 45°. The oblique incidence has little influence on the scattering cancellation performance and absorption performance, which is attributed to the intrinsic characteristic of crossed dipole structure.

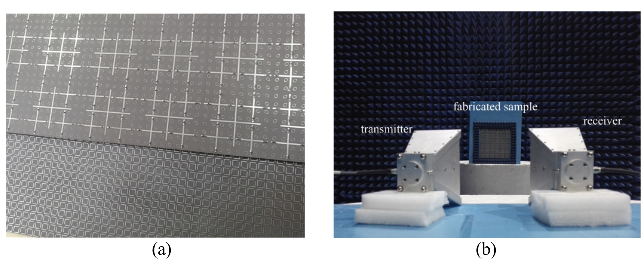

FIGURE 11. The photographs of (a) fabricated sample and (b) measurement setup.

B. FABRICATION AND MEASUREMENT

To verify the designed tri-band RCS reduction experimentally, a metasurface sample was fabricated using printed circuit board technology and measured in the microwave anechoic chamber, as shown in Fig. 11. The fabricated sample occupies 288×288 mm^2, following the model used in the simulation. The top and bottom layers are depicted in the upper half and lower half parts of Fig. 11(a), respectively. Moreover, the top layer is stacked above the bottom layer by glue. The glue layer was only applied on the four corners of the square sample, and its thickness is too thin to consider the influence. The specular reflection was measured by using free space method in anechoic chamber. As shown in Fig. 11(b), a pair of wideband horn antennas was used as transmitter and receiver and connected to the two ports of vector network analyzer (AV 3672B). The time-domain gating function in the network analyzer was used to eliminate the interference of the environment in the measurement. Hence, the reflection of the metasurface can be evaluated by the transmission coefficient S_{12} of two horn antennas. The transmitter and receiver were tilted at an angle of 5° about the normal direction of sample to prevent the interference effect between incident and reflected waves. A metallic plate with the same size was also measured as a reference to show the reflection suppression of the designed metasurface. The reflection was measured up to 18 GHz due to the limitation of the measurement condition. To provide a clear insight of the comparison of measured and simulated results, the results are separated into two frequency ranges, as shown in Figs. 12(a) and (b), respectively. As expected, tri-band RCS reduction can be realized for both x- and y-polarized incidence. The measured results coincide well with the simulated results, except for the discrepancy in the absorption band, which can be attributed to the imperfect soldering of embedded resistors. In addition, the difference between real and assumed characteristic values of the F4B dielectric substrate and misalignment of distinction are other reasons for the distinction between simulated and measured RCS reduction spectrums. Nevertheless, tri-band RCS reduction has been experimentally verified in a reasonable manner.

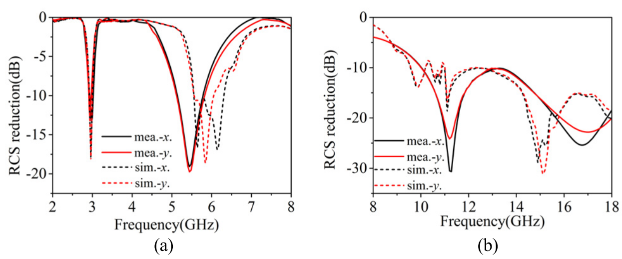

FIGURE 12. The measured RCS reductions under normally incidence for both x-polarized and y-polarized at (a) 2-8 GHz and (b) 8-18 GHz.

V. CONCLUSION

In this study, a tri-band metasurafce for RCS reduction was designed, fabricated and measured. The reduction mechanisms in three operational bands are different. The RCS from X-band to K-band was suppressed by randomly distributing polarization rotatable unit cells. The C-band RCS reduction was attributed to the absorption of incoming wave. Moreover, the scattering cancellation is a reason for RCS reduction in S-band. The RCS reduction performance in each band is independent to each other due to the different mechanisms, leading to conveniently manipulation of operational band as desired. With the increment of incidence angle, the tri-band RCS reduction can be still achieved until the incidence angle up to 45°, proving the angle stability of the metasurface. The agreement between simulated and measured results reveals the feasibility of the proposed metasurface.

REFERENCES

[1] E. F. Knott, M. T. Tuley, and J. F. Shaeffer, *Radar Cross Section*, 2nd ed. Norwood, MA, USA: Artech House, 1993.
[2] N. Yu *et al.*, "Light propagation with phase discontinuities: Generalized laws of reflection and refraction," *Science*, vol. 334, no. 6054, pp. 333–337, Oct. 2011.
[3] N. K. Grady *et al.*, "Terahertz metamaterials for linear polarization conversion and anomalous refraction," *Science*, vol. 340, no. 6138, pp. 1304–1307, 2013.
[4] M. L. N. Chen, L. J. Jiang, and W. E. I. Sha, "Artificial perfect electric conductor-perfect magnetic conductor anisotropic metasurface for generating orbital angular momentum of microwave with nearly perfect conversion efficiency," *J. Appl. Phys.*, vol. 119, no. 6, p. 064506, 2016.
[5] N. I. Landy, S. Sajuyigbe, J. J. Mock, D. R. Smith, and W. J. Padilla, "Perfect metamaterial absorber," *Phys. Rev. Lett.*, vol. 100, p. 207402, May 2008.
[6] W. Yuan and Y. Cheng, "Low-frequency and broadband metamaterial absorber based on lumped elements: Design, characterization and experiment," *Appl. Phys. A*, vol. 117, no. 4, pp. 1915–1921, 2014.
[7] D. Kundu, A. Mohan, and A. Chakrabarty, "Single-layer wideband microwave absorber using array of crossed dipoles," *IEEE Antennas Wireless Propag. Lett.*, vol. 15, pp. 1589–1592, 2016.
[8] Y. J. Kim *et al.*, "Ultrathin microwave metamaterial absorber utilizing embedded resistors," *J. Phys. D, Appl. Phys.*, vol. 50, no. 40, p. 405110, 2017.
[9] M. Paquay, J. C. Iriarte, I. Ederra, R. Gonzalo, and P. D. Maagt, "Thin AMC structure for radar cross-section reduction," *IEEE Trans. Antennas Propag.*, vol. 55, no. 12, pp. 3630–3638, Dec. 2007.
[10] A. Edalati and K. Sarabandi, "Wideband, wide angle, polarization independent RCS reduction using non absorptive miniaturized element frequency selective surfaces," *IEEE Trans, Antennas Propag.*, vol. 62, no. 2, pp. 747–754, Feb. 2014.
[11] W. Chen, C. A. Balanis, and C. R. Birtcher, "Checkerboard EBG surfaces for wideband radar cross section reduction," *IEEE Trans. Antennas Propag.*, vol. 63, no. 6, pp. 2636–2645, Jun. 2015.
[12] Y.-Q. Zhuang, G.-M. Wang, and H.-X. Xu, "Ultra-wideband RCS reduction using novel configured chessboard metasurface," *Chin. Phys. B*, vol. 26, no. 5, p. 054101, 2017.
[13] A. Y. Modi, C. A. Balanis, C. R. Birtcher, and H. N. Shaman, "Novel design of ultra-broadband radar cross section reduction surfaces using artificial magnetic conductors," *IEEE Trans. Antennas Propag.*, vol. 65, no. 10, pp. 5406–5417, Oct. 2017.
[14] J. Chen, Q. Cheng, J. Zhao, D. S. Dong, and T. J. Cui, "Reduction of radar cross section based on a metasurface," *Prog. Electromagn. Res.*, vol. 146, pp. 71–76, 2014.
[15] L. H. Gao *et al.*, "Broadband diffusion of terahertz waves by multi-bit coding metasurfaces," *Light Sci. Appl.*, vol. 4, p. e324, Sep. 2015.
[16] D. S. Dong *et al.*, "Terahertz broadband low-reflection metasurface by controlling phase distributions," *Adv. Opt. Mater.*, vol. 3, no. 10, pp. 1405–1410, 2015.
[17] J. Su *et al.*, "Fast analysis and optimal design of metasurface for wideband monostatic and multistatic radar stealth," *J. Appl. Phys.*, vol. 120, no. 20, p. 205107, 2016.
[18] X. Yan *et al.*, "Broadband, wide-angle, low-scattering terahertz wave by a flexible 2-bit coding metasurface," *Opt. Exp.*, vol. 23, no. 22, pp. 29128–29137, Nov. 2015.
[19] Y. Zhang *et al.*, "Broadband diffuse terahertz wave scattering by flexible metasurface with randomized phase distribution," *Sci. Rep.*, vol. 6, p. 26875, May 2016.
[20] J. Zhao *et al.*, "Achieving flexible low-scattering metasurface based on randomly distribution of meta-elements," *Opt. Exp.*, vol. 24, no. 24, pp. 27849–27857, Nov. 2016.
[21] K. Chen, L. Cui, Y. Feng, J. Zhao, T. Jiang, and B. Zhu, "Coding metasurface for broadband microwave scattering reduction with optical transparency," *Opt. Exp.*, vol. 25, no. 5, pp. 5571–5579, Mar. 2017.

[22] Y. Zhuang, G. Wang, J. Liang, T. Cai, W. Guo, and Q. Zhang, "Flexible and polarization-controllable diffusion metasurface with optical transparency," *J. Phys. D, Appl. Phys.*, vol. 50, no. 46, p. 465102, 2017.
[23] M. Moccia *et al.*, "Coding metasurfaces for diffuse scattering: Scaling laws, bounds, and suboptimal design," *Adv. Opt. Mater.*, vol. 5, no. 19, p. 1700455, 2017.
[24] K. Wang, J. Zhao, Q. Cheng, D. S. Dong, and T. J. Cui, "Broadband and broad-angle low-scattering metasurface based on hybrid optimization algorithm," *Sci. Rep.*, vol. 4, p. 5935, Aug. 2014.
[25] Y. Zhao *et al.*, "Broadband diffusion metasurface based on a single anisotropic element and optimized by the Simulated Annealing algorithm," *Sci. Rep.*, vol. 6, p. 23896, Apr. 2016.
[26] H. Zhang, Y. Lu, J. Su, Z. Li, J. Liu, and Y. Yang, "Coding diffusion metasurface for ultra-wideband RCS reduction," *Electron. Lett.*, vol. 53, no. 3, pp. 187–189, Feb. 2017.
[27] Y. Zhuang *et al.*, "Random combinatorial gradient metasurface for broadband, wide-angle and polarization-independent diffusion scattering," *Sci. Rep.*, vol. 7, p. 16560, Nov. 2017.
[28] W. Chen, C. A. Balanis, and C. R. Birtcher, "Dual wide-band checkerboard surfaces for radar cross section reduction," *IEEE Trans. Antennas Propag.*, vol. 64, no. 9, pp. 4133–4138, Sep. 2016.
[29] Y. Cheng *et al.*, "An ultra-thin dual-band phase-gradient metasurface using hybrid resonant structures for backward RCS reduction," *Appl. Phys. B*, vol. 123, p. 143, May 2017.
[30] Y. Zhuang, G. Wang, J. Liang, and Q. Zhang, "Dual-band low-scattering metasurface based on combination of diffusion and absorption," *IEEE Antennas Wireless Propag. Lett.*, vol. 16, pp. 2606–2609, 2017.
[31] S. Kirkpatrick, C. D. Gelatt, and M. P. Vecchi, "Optimization by simulated annealing," *Science*, vol. 220, no. 4598, pp. 671–680, 1983.
[32] S. J. Li *et al.*, "Ultra-broadband reflective metamaterial with RCS reduction based on polarization convertor, information entropy theory and genetic optimization algorithm," *Sci. Rep.*, vol. 6, p. 37409, Nov. 2016.

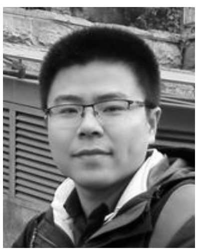

YAQIANG ZHUANG was born in Quanzhou, Fujian, China, in 1990. He received the B.S. degree in radar engineering from Air Force Engineering University, Xi'an, China, in 2012, and the B.S. degree in electromagnetic field and microwave technology in 2014, where he is currently pursuing the Ph.D. degree.

He has authored over 10 peer-viewed first-author papers in *Optics Express*, *Scientific Reports*, *Journal of Physics D: Applied Physics*, the IEEE Antennas and Wireless Propagation Letters, *Chinese Physics B*, and so on. His current research interests include metasurface, and their applications to radiation and scattering platforms.

Dr. Zhuang served as a Reviewer of the IEEE Transactions on Antennas and propagations and the IEEE Access.

GUANGMING WANG (M'17) was born Dangshan, Anhui, China, in 1964. He received the B.S. and M.S. degrees from the Air Force Engineering University, Xi'an, China, in 1984 and 1990, respectively, and the Ph.D. degree from the University of Electronic Science and Technology, Chengdu, China, in 1994, all in electromagnetic field and microwave technology.

He joined the Air Force Engineering University as an Associate Professor, was promoted to a Full Professor in 2000, and is now the Head of the Microwave Laboratory. He has authored and coauthored more than 150 conference and journal papers. His current interests include microwave circuits, antennas, and also the new structures including EBG, PBG, metamaterials, fractals, etc.

Prof. Wang has been a Senior Member of the Chinese Institute of Electronics. From 1994 to date, he was awarded and warranted several items supported under the National Natural Science Foundation of China and fulfilled many local scientific research programs.

QINGFENG ZHANG (S'07–M'11–SM'15) was born in Changzhou, Jiangsu, China, in 1984. He received the B.E. degree in electrical engineering from the University of Science and Technology of China, Hefei, China, in 2007, and the Ph.D. degree in electrical engineering from Nanyang Technological University, Singapore, in 2011.

From 2011 to 2013, he was with the Poly-Grames Research Center, École Polytechnique de Montréal, Montreal, QC, Canada, as a Post-Doctoral Fellow. Since 2013, he has been with the Southern University of Science and Technology, Shenzhen, China, as an Assistant Professor. His current research interests include emerging novel electromagnetics technologies and multidisplininary topics.

Dr. Zhang was a recipient of the Shenzhen Overseas High-Caliber Personnel in 2014, the Guangdong Natural Science Funds for Distinguished Young Scholar in 2015, the Shenzhen Nanshan Piloting Talents in 2016, and the Guangdong Special Support Program for Top-Notch Young Talents in 2017. He was a Lead Guest Editor of the *International Journal of Antennas and Propagation* from 2014 to 2015, and the Publication Chair at the IEEE International Conference on Communication Systems in 2016.

CHENG ZHOU was born in Chizhou, Anhui, China, in 1989. He received the B.E., M.S., and Ph.D. degrees in electromagnetic field and microwave technology from Air Force Engineering University, Xi'an, China, in 2009, 2011, and 2016, respectively.

Since 2016, he has been with the Unit 95899 of CPLA, Beijing, China, as an Engineer. His current research interests include radio communication and orbital angular momentum.